Complex Dynamic Features of a Cooled Reverse-Flow Reactor

J. Khinast, A. Gurumoorthy, and D. Luss
Dept. of Chemical Engineering, University of Houston, Houston, TX 77204

A reverse-flow reactor (RFR) usually attains a symmetric period-1 state, so that the temperature profile just after a flow reversal is a mirror image of that after the previous flow reversal. Recent simulations show that in certain cases a cooled RFR may attain other states with different types of periodicity or even complex quasi-periodic states. The maximum temperature of these states often exceeds that of the symmetric states so that it may deactivate the catalyst and/or lead to safety problems. A systematic, numerically efficient method is presented for constructing maps of parameter regions in which a cooled RFR has qualitatively different dynamic features. The technique is applied to determine the dependence of these dynamic features on the cooling capacity and flow-reversal period. Stable quasi-periodic and asymmetric period-1 states exist mainly for short flow-reversal periods. The quasi-periodic states usually exist for lower cooling capacities than those for which the asymmetric period-1 states exist. Stable symmetric and asymmetric period-1 states exist for the same set of parameters in very narrow regions of the parameter space. The behavior of the RFR in the limit of very fast flow reversals is usually modeled by a countercurrent flow reactor, with equal flow rates in the two compartments. This cooled reactor may attain asymmetric states for certain sets of parameters.

Introduction

A reverse-flow reactor (RFR) is a packed-bed reactor in which the flow direction is periodically reversed (Figure 1) to trap a hot zone within the reactor. It is one of the only two continuous, periodic, heterogeneous catalytic processes that have found technological applications so far (the second is the circulating fluidized bed). The RFR concept was proposed and patented by Cottrell (1938) for removal of pollutants. Frank-Kamenetskii (1955) described the oxidation of isopropyl-alcohol to acetone over a copper catalyst in an RFR. The recent applications and interest in RFR have been motivated by its successful application to SO_2 oxidation in Russia (Boreskov et al., 1979; Boreskov and Matros, 1983). A patent for reduction of SO_2 in an RFR was issued to Watson (1975). Experimental investigations include the removal of nitrogen oxides (Bobrova et al., 1988), production of syngas (Blanks et al., 1990), methanol synthesis (Neophytides and Froment, 1992), the catalytic combustion of VOCs (Nieken et al., 1994; van de Beld, 1995), and catalytic oxidation of CO (Züfle and Turek, 1997). A comprehensive review of the applications and studies of the RFR was presented by Matros and Bunimovich (1996).

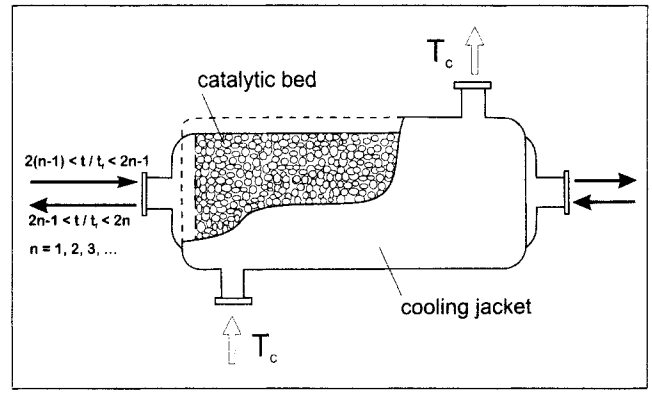

Figure 1. Cooled reverse-flow reactor.

The rational design and operation of an RFR require efficient prediction of its performance. Dynamic simulations of

Correspondence concerning this article should be addressed to D. Luss.

an RFR are usually rather lengthy as the periodic states are attained only after several hundreds of flow reversals (Nieken et al., 1995). This motivated the analysis of limiting models which predict its features for very short and infinite long flow reversal periods (Eigenberger and Nieken, 1988; Matros, 1990; Nieken et al., 1995; Somani et al., 1997). The computational effort of solving the full model may be considerably reduced by the procedure proposed by Gupta and Bhatia (1991) of calculating directly the periodic solutions by forcing the temperature profile after a flow-reversal period (half cycle) to be a mirror image of the original one. Thus, the set of partial differential equations is solved as a spatial and temporal boundary-value problem.

The RFR operates under conditions for which in addition to the extinguished (low temperature) state at least one periodic state exists with a hot zone trapped in the reactor. Chumakova and Matros (1991) showed that the model of an RFR in which a single reaction occurs has three periodic solutions, at least one of them unstable. Ivanov et al. (1992) and Salinger and Eigenberger (1996b) have shown that up to five periodic solutions (two of them unstable) may exist for some parameters for a model of an RFR in which two independent, exothermic reactions occur. Nieken et al. (1994) observed this multiplicity during the simultaneous oxidation of propylene and propane.

Information about the impact of the operating and design conditions (parameters) on the periodic states of an RFR is usually presented in the form of bifurcation diagrams. At first, numerical simulations were used to construct these bifurcation diagrams (Matros, 1990; Bhatia, 1991; Gupta and Bhatia, 1991; Sapundzhiev et al., 1993; Snyder and Subramaniam, 1993; van de Beld and Westerterp, 1994; van de Beld, 1995; Nieken et al., 1995; Seiler and Emig, 1997). Chumakova and Matros (1991) used the catastrophe theory to find isolated branches in the bifurcation diagrams of conversion vs. the superficial flow velocity for the limiting model of very short flow-reversal periods. Recently, Salinger and Eigenberger (1996a,b) used a numerical continuation technique to track limit points of a two-phase model of an RFR in which either one or two independent reactions occurred and determined parameter regions with different numbers of solutions. Khinast and Luss (1997) developed a systematic, numerically efficient procedure for mapping parameter regions with qualitatively different bifurcation diagrams of the RFR. The efficiency of their numerical procedure was due to direct application of the singularity theory to the infinite dimensional model, shooting in time, continuation techniques, and Broyden's method, which circumvents repeated computation of the Jacobian matrix.

Salinger and Eigenberger (1996a,b) and Khinast and Luss (1997) found that, in general, an adiabatic RFR attains only symmetric states and that $q+1$ of the $2q+1$ periodic states are stable. Numerical simulations by Rehacek et al. (1992, 1998) showed that a cooled RFR may have complex and aperiodic states. Simulations by Salinger and Eigenberger (1996b) supported some of these findings suggesting that cooling causes the intricate dynamic behavior. The stability of the symmetric periodic states may be analyzed by Floquet theory (Iooss and Joseph, 1990), that is, by computing the eigenvalues of the monodromy matrix. This method has been applied to various periodic systems in the chemical engineering literature (Kevrekidis et al., 1986; Gogolides et al., 1992; Croft and LeVan, 1994a,b; Salinger and Eigenberger, 1996a,b).

In some industrial applications an RFR has to be cooled in order to avoid catalyst damage or undesired reactions. Additionally, it is extremely difficult to avoid heat losses in laboratory and pilot reactors. The objective of this work is to map parameter regions in which a cooled RFR exhibits qualitatively different dynamic features. These maps determine, among others, the parameter regions in which asymmetric and quasi-periodic states exist. A systematic and numerically efficient method is presented for constructing these maps. It does not require determination of the eigenvalues of the monodromy matrix, thus greatly reducing the computational effort. This methodology is used to determine the dynamics of a specific example in order to gain insight and understanding of the conditions leading to the various dynamic features of a cooled RFR.

The dynamic behavior of an RFR in the limit of very fast flow reversals is usually modeled by a countercurrent flow reactor, with equal flow rates in the two compartments. It is usually assumed that the reactor attains symmetric states. We show that the limiting model also has asymmetric solutions for certain parameters. Moreover, this limiting model predicts states, which differ from those of the full model for extremely high flow-reversal frequencies.

Model of the Cooled RFR

We consider a cooled RFR in which a single irreversible, exothermic, first-order reaction occurs. We describe the RFR by a one-dimensional, pseudo-homogeneous model that accounts for axial heat and mass dispersion and external mass-transfer resistance between the fluid and the catalyst. The model assumes that all the physical properties are independent of the temperature and concentration and that the effective axial thermal conductivity λ_{ax} (W/m·K) satisfies the relation (Vortmeyer and Schäfer, 1974)

$$\lambda_{ax} = (1-\epsilon)\lambda_s + \lambda_{sg} \tag{1}$$

where

$$\lambda_{sg} = \frac{u^2(\rho c_p)_g^2}{h a_v}. \tag{2}$$

The conductivity of the solid phase and the effective thermal dispersion due to the heat transfer between the solid and the gas are accounted for by the first and the second term in Eq. 1, respectively. Chen and Luss (1989) showed that the predictions of the pseudo-homogeneous model and a two-phase model are generally very similar when the temperature front moves downstream. This model has been used to simulate the dynamic features of an RFR by several authors (Eigenberger and Nieken, 1988; Matros, 1989; Haynes et al., 1995; Nieken et al., 1995; Seiler and Emig, 1997; Khinast and Luss, 1997).

The dimensionless energy and species balances describing the temperature Θ and conversion x are

$$\frac{Le}{\sigma}\frac{\partial\Theta}{\partial\tau}-\frac{1}{\phi_h^2}\frac{\partial^2\Theta}{\partial\xi^2}+\frac{f}{Da}\frac{\partial\Theta}{\partial\xi}-\beta\cdot B(\Theta)\cdot(1-x)+\Delta\cdot(\Theta-\Theta_c)=0$$

$$\frac{\epsilon}{\sigma}\frac{\partial x}{\partial\tau}-\frac{1}{\phi_m^2}\frac{\partial^2 x}{\partial\xi^2}+\frac{f}{Da}\frac{\partial x}{\partial\xi}-B(\Theta)\cdot(1-x)=0 \quad (3)$$

The dimensionless variables

$$x=\frac{c_0-c}{c_0},\quad \Theta=\frac{T}{T_0},\quad \tau=\frac{t}{t_f},\quad \xi=\frac{z}{L}, \quad (4)$$

depend on the dimensionless groups

$$\Psi=\frac{(\rho c_p)_s}{(\rho c_p)_g},\quad Le=\Psi(1-\epsilon)+\epsilon,\quad \sigma=t_f\cdot k(T_0),$$

$$\Theta_c=\frac{T_c}{T_0},\quad \phi_h^2=\frac{L^2k(T_0)(\rho c_p)_g}{\lambda_{ax}},$$

$$\phi_m^2=\frac{L^2k(T_0)}{\epsilon D_{ax}},\quad \Delta=\frac{2U}{r(\rho c_p)_g k(T_0)},\quad \gamma=\frac{E_a}{RT_0}$$

$$Da=\frac{Lk(T_0)}{u},\quad \beta=\frac{\Delta T_{ad}}{T_0},\quad B(\Theta)=\frac{a_v k_c\exp\left[\gamma\left(\frac{\Theta-1}{\Theta}\right)\right]}{a_v k_c+k_\infty\exp\left[-\frac{\gamma}{\Theta}\right]} \quad (5)$$

where

$$k(T_0)=k_\infty\cdot\exp\left[-\frac{E_a}{RT_0}\right] \quad (6)$$

The flow direction indicator f in Eq. 3 is equal to 1 (-1) for flow from the left (right). The flow direction is reversed at each multiple of the *flow-reversal period* t_f, that is, at $\tau=1, 2, 3, \ldots, n$. Each *cycle* consists of two flow-reversals, that is

$$t_c=2\cdot t_f \quad \text{or} \quad \tau_c=2 \quad (7)$$

The spatial boundary conditions for the flow from the left to the right ($f=1$) are

$$\frac{Da}{\phi_h^2}\frac{\partial\Theta}{\partial\xi}=(\Theta-1),\quad \frac{Da}{\phi_m^2}\frac{\partial x}{\partial\xi}=x \quad \text{at} \quad \xi=0 \quad (8)$$

$$\frac{\partial\Theta}{\partial\xi}=0,\quad \frac{\partial x}{\partial\xi}=0 \quad \text{at} \quad \xi=1 \quad (9)$$

This set of partial differential equations and boundary conditions may be written in the vectorial form

$$\boldsymbol{g}(\boldsymbol{u},\lambda,\boldsymbol{p})=\boldsymbol{0},\quad \boldsymbol{u}(\xi,\tau)^T=[\Theta(\xi,\tau),x(\xi,\tau)] \quad (10)$$

Table 1. Parameters Used in the Simulations

$T_0=T_c$	323 K	E_a/R	8,328.6 K
k_∞	1.815×10^7 s^{-1}	k_c	0.115 m/s
$(\rho c_p)_g$	0.6244 kJ/m^3·K	$(\rho c_p)_s$	1,318.61 kJ/m^3 K
a_v	2,628.8 m^2_{Surf}/m^3_{React}	L	1.0 m
u	2.0 m/s	λ_s	1.26 W/m·K
h	0.13 kW/m^2·K	ϵ	0.69
D_{eff}	4×10^{-5} m^2/s	ΔT_{ad}	50 K

We illustrate now some behavioral features of the RFR. The parameters used in the simulations are reported in Table 1. The kinetic parameters correspond to the catalytic oxidation of propane (Nieken and Eigenberger, 1988).

For a flow-reversal period of 60 s the corresponding dimensionless groups are

$$Le=686.6,\quad \Psi=2212.7,\quad \sigma=6.9\times10^{-3},$$
$$Da=5.745\times10^{-5},\quad \phi_h^2=1.4482\times10^{-2},\quad \phi_m^2=4.16,$$
$$\beta=0.155,\quad \gamma=25.785 \quad (11)$$

Figure 2 shows a typical dependence of the maximum RFR temperature on the cooling capacity Δ for the parameter set in Eq. 11. An ignited state of a cooled RFR exists only if the cooling capacity does not exceed a critical value, which increases as the adiabatic temperature rise of the reaction increases. An extinguished state exists for all physical cooling capacities ($\Delta\geq0$). The branch of the extinguished states emanates from a bifurcation point with a negative cooling capacity. Clearly, states corresponding to negative Δ values have no physical meaning and are not encountered in practice. Note that the maximum temperature of the ignited states exhibits a nonmonotonic dependence on the cooling capacity. Quasi-periodic states exist in this case in a region where the maximum temperature of the symmetric states on the ignited branch has a local minimum. The maximum temperature of the quasi-periodic states exceeds those of the symmetric ones. The nonmonotonic dependence of the cooling capacity is best

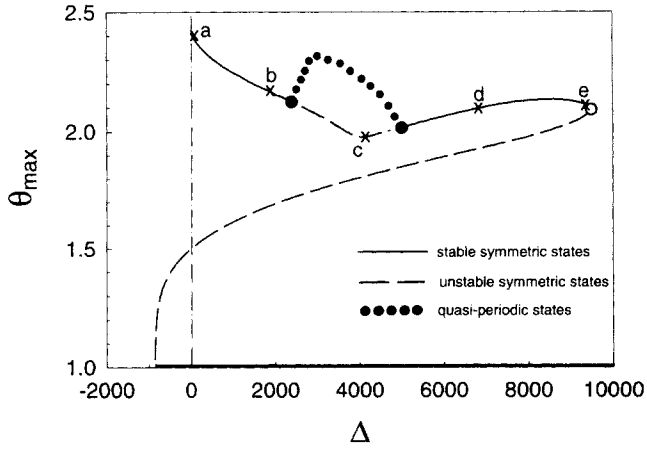

Figure 2. Typical dependence of the maximum RFR temperature Θ_{max} on the cooling capacity Δ.
Letters denote states shown in Figure 3.

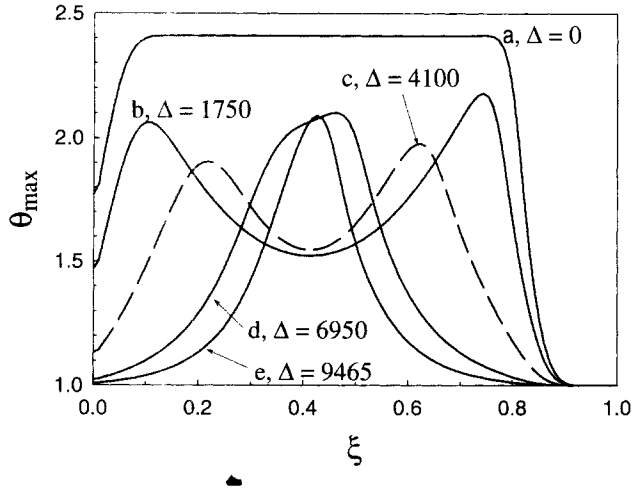

Figure 3. Temperature profiles as the flow is switched from the left to the right for symmetric period-1 states obtained for different cooling capacities Δ.

Unstable profiles are shown by a dashed line; letters refer to marked states in Figure 2.

understood by inspection of some temperature profiles (Figure 3) when the flow direction is reversed from the right to the left. The corresponding states are marked in Figure 2. The combination of cooling and the relative fast flow-reversal frequency initially generates a hot zone with two temperature peaks (Figures 3b and 3c). Approaching the extinction point, the hot region shrinks as the cooling capacity increases. This causes a shift to a hot zone with only one temperature maximum (Figures 3d and 3e). Following the transition from two temperature peaks to one temperature peak the maximum temperature increases with increasing cooling capacity.

Various dynamic features of a cooled RFR are illustrated in Figure 4, which shows a time series of the dimensionless temperature Θ_m in the middle of the fixed bed ($\xi = 0.5$) vs. the dimensionless time. Note that a full cycle consists of two flow reversals, that is, $\tau_c = 2$. Case a describes the most common behavior of an RFR, that is, a symmetric period-1 operation. The corresponding temperature profile (Figure 5a) has two maxima. Thus, the time series has two maxima in each flow-reversal period. When the cycle time is reduced and the cooling capacity increased, an asymmetric period-1 behavior may be observed such as that shown in Figure 4b. The corresponding temperature profiles are shown in Figure 5b. Figure 4c illustrates a quasi-periodic motion in which the reactor returns approximately (but not exactly) to its original state after approximately 200 flow-reversals (100 cycles). Figure 4d shows a more complicated quasi-periodic motion with a faster second frequency for the same cooling capacity and a longer flow-reversal period. In this case, the reaction heat accumulates in different regions of the reactor and the hot zone moves slowly (Figure 5d). We did not find parameters that generated chaotic motion. However, chaotic states may be attained for other reaction systems and parameter sets (Rehacek et al., 1992, 1998).

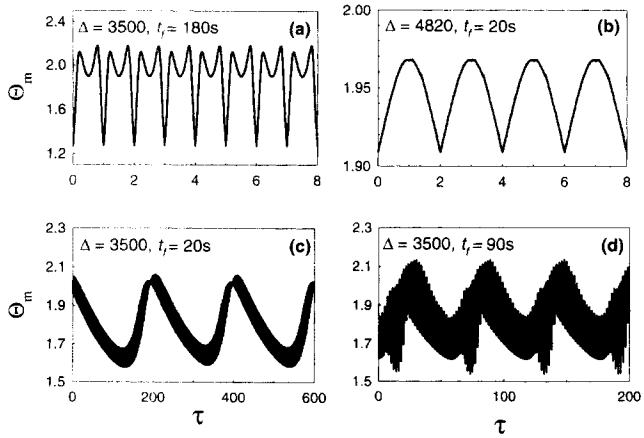

Figure 4. Influence of the cooling capacities Δ and flow-reversal period t_f on the time series of the temperature at the center of a cooled RFR.

(a) Symmetric period-1 state; (b) asymmetric period-1 state; (c) and (d) quasi-periodic states.

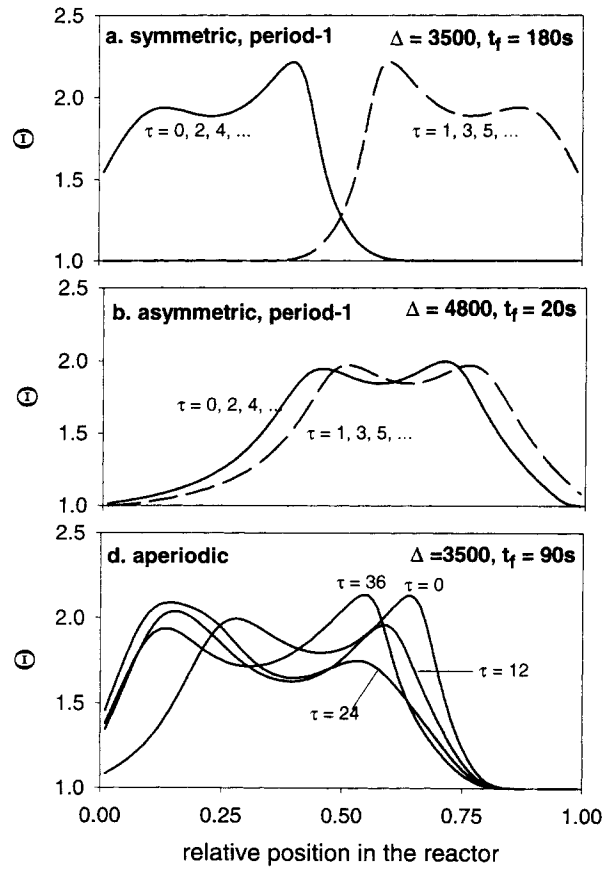

Figure 5. Temperature profiles of cases (a, b, d) in Figure 4 as the flow direction is switched from the left to the right.

(a) Symmetric period-1 state; (b) asymmetric period-1 state; (d) quasi-periodic state.

Bounding Regions with Asymmetric or Aperiodic Motion

We describe here the mathematical background and the numerical technique for computing the loci separating parameter regions with different dynamic features. This tech-

nique is applied in the next section to map the parameter regions leading to the complex dynamics and to gain an understanding of these surprising dynamics.

Khinast and Luss (1997) presented an efficient numerical scheme for the determination of the multiplicity features of an RFR. The method was based on construction of loci of codimension-1 singular points of the symmetric period-1 states in the plane of two operating or design variables by direct application of the singularity theory to the infinite dimensional model. The numerical method combined *shooting* in time, *continuation* techniques and the *Broyden's method* to enable fast tracking of the bifurcations by avoiding repeated computation of the Jacobian matrix.

The most efficient computation of a symmetric, periodic state of an RFR was suggested by Gupta and Bhatia (1991). It converts the model equations into a boundary value problem (BVP) by enforcing the symmetry of the profiles after one flow reversal. Specifically, for a symmetric period-1 state solution of this BVP requires the vanishing of the *residual function* at $\tau = 1$.

$$\boldsymbol{F}^s(\boldsymbol{u}_0, \lambda, \boldsymbol{p}) = \boldsymbol{u}_0 - \tilde{\boldsymbol{u}}(\tau = 1). \tag{12}$$

Here $\boldsymbol{u}_0$ and $\tilde{\boldsymbol{u}}(1)$ are the spatially discretized state variables at $\tau = 0$ and $\tau = 1$, respectively, that is, the vectors of the temperature and conversion at each node point. The tilde denotes mirror reflection, that is, it maps ξ into $1 - \xi$ and the superscript s denotes a semi-cycle. The residual function for a full cycle with a period of $\tau = 2$ is

$$\boldsymbol{F}^c(\boldsymbol{u}_0, \lambda, \boldsymbol{p}) = \boldsymbol{u}_0 - \boldsymbol{u}(\tau = 2) \tag{13}$$

The superscript c denotes a cycle consisting of two flow reversals.

The method described below finds efficiently the solutions of these two residual functions. The finding of $\boldsymbol{u}_0$, for which the residual function defined by Eq. 12 vanishes, yields the symmetric states of period 1. The vanishing of Eq. 13 determines both symmetric and asymmetric period-1 states. The numerical method consists of assuming a vector of the variables at all the node points at $\tau = 0$, that is, $\boldsymbol{u}_0$, and integrating the model equations, Eq. 3, by an initial value problem (IVP) solver. A Newton-Raphson method uses the residual to converge to $\boldsymbol{u}_0$. We found that the method of finite differences with upwinding of the first derivatives in the mass balance gave a smaller discretization error than orthogonal collocation on finite elements. Grid refinement studies showed that the use of 100 spatial node points yielded sufficient accuracy. Details of the shooting method are described by Khinast and Luss (1997).

We extend here the previous method of predicting changes in the multiplicity features of a periodic system to determine the loci of the following dynamic bifurcations: transition from a symmetric to an asymmetric periodic state, shift to quasi-periodic dynamics, and transition to a period-q behavior.

The stability of a periodic state depends on the spectrum of the eigenvalues of the *monodromy matrix* $\boldsymbol{M}$ of the periodic solutions, that is, the matrix, which reflects the propagation of small perturbations over one cycle (Coddington and Levinson, 1955; Iooss and Joseph, 1980). Generically, a periodic state is stable when the absolute value of every eigenvalue (*Floquet multiplier*) of the monodromy matrix is smaller than unity. A periodic solution becomes unstable when one eigenvalue crosses the unit circle. Different bifurcations occur depending on the angle at which the eigenvalues cross the unit circle.

In principle, it is possible to track the various bifurcations by repeatedly computing the monodromy matrix and its eigenvalues. In practice, repeated computation of the monodromy matrix requires extensive computer capacity and time. This led us to develop an alternative method for tracking the dynamic bifurcations. In some cases we computed $\boldsymbol{M}$ and the Floquet multipliers in order to check the validity of the stability predictions. The numerical procedure for determining $\boldsymbol{M}$ is described in the Appendix.

One advantage of our method for predicting changes in the multiplicity features of the periodic states is the elimination of the need to compute the Jacobian matrix. We only need to determine the product of the Jacobian matrix with its eigenvector. The same concept is exploited in this study by finding first a relation between the monodromy matrix and the Jacobian matrix. Consequently, the defining conditions of the various singularities do not require computation of either the monodromy or the Jacobian matrix.

In a sufficient close neighborhood of u_0 and λ_0 a small perturbation $\delta \boldsymbol{u}_k$ of a symmetric solution $\boldsymbol{u}_0$ is governed by

$$\delta \tilde{\boldsymbol{u}}_{k+1} = \boldsymbol{M}^s(\boldsymbol{u}_0, \lambda_0) \cdot \delta \boldsymbol{u}_k \tag{14}$$

The Jacobian matrix $\boldsymbol{J}^s$ of the residual function defined by Eq. 12 is

$$\begin{aligned} \boldsymbol{J}^s(\boldsymbol{u}_0, \lambda_0) \cdot \delta \boldsymbol{u}_k &= \boldsymbol{F}^s(\boldsymbol{u}_0 + \delta \boldsymbol{u}_k, \lambda_0) - \boldsymbol{F}^s(\boldsymbol{u}_0, \lambda_0) \\ &= \left\{\boldsymbol{u}_0 + \delta \boldsymbol{u}_k - \left[\tilde{\boldsymbol{u}}(\tau_f) + \delta \tilde{\boldsymbol{u}}_{k+1}\right]\right\} - \left[\boldsymbol{u}_0 - \tilde{\boldsymbol{u}}(\tau_f)\right] \\ &= \delta \boldsymbol{u}_k - \delta \tilde{\boldsymbol{u}}_{k+1} \end{aligned} \tag{15}$$

Equations 14 and 15 give

$$\boldsymbol{M}^s(\boldsymbol{u}_0, \lambda_0) = \frac{\delta \tilde{\boldsymbol{u}}_{k+1}}{\delta \boldsymbol{u}_k} = \boldsymbol{I} - \boldsymbol{J}^s(\boldsymbol{u}_0, \lambda_0) \tag{16}$$

Similarly

$$\boldsymbol{M}^c(\boldsymbol{u}_0, \lambda_0) = \frac{\delta \boldsymbol{u}_{k+1}}{\delta \boldsymbol{u}_k} = \boldsymbol{I} - \boldsymbol{J}^c(\boldsymbol{u}_0, \lambda_0) \tag{17}$$

Equations 16 and 17 establish a relation between the monodromy matrix and the Jacobian (linearization) of the residual equations. These relations are essential for tracking the dynamic singular points.

At a *limit point of a symmetric state* (L-S) one eigenvalue of $\boldsymbol{M}^s$ crosses the unit circle at $\mu = +1$. At a *limit point of an asymmetric state* (L-AS) one eigenvalue of $\boldsymbol{M}^c$ is $\mu = +1$. A symmetric period-1 solution undergoes a *symmetry loss* (SL) bifurcation when $\boldsymbol{M}^s$ has a $\mu = -1$ eigenvalue. A *period doubling* (PD) bifurcation occurs when $\boldsymbol{M}^c$ has a $\mu = -1$ eigenvalue. When a conjugate complex pair of eigenvalues crosses the unit circle a quasi-periodic (two-torus) state is

usually obtained. We denote the *bifurcation of quasi-periodic solutions* from symmetric (asymmetric) ones as QP-S (QP-AS). Each of the described bifurcations satisfies the condition

$$\boldsymbol{M}\boldsymbol{v}_0 = (\boldsymbol{I} - \boldsymbol{J})\boldsymbol{v}_0 = \mu\boldsymbol{v}_0 \tag{18}$$

where

$$Re(\mu)^2 + Im(\mu)^2 = 1 \tag{19}$$

We rewrite Eq. 18 for one or two flow-reversal periods as

$$\boldsymbol{J}^s\boldsymbol{v}_0 = (1-\mu)\cdot\boldsymbol{v}_0 \quad \text{or} \quad \boldsymbol{J}^c\boldsymbol{v}_0 = (1-\mu)\cdot\boldsymbol{v}_0 \tag{20}$$

As in Khinast and Luss (1997), we use the fact that the product of the Jacobian matrix with its eigenvector can be determined by direct Fréchet differentiation of the residual Eqs. 12 or 13

$$\boldsymbol{D}_u\boldsymbol{F}^s(\boldsymbol{u}_0, \lambda)\cdot\boldsymbol{v}_0 = \boldsymbol{J}^s\cdot\boldsymbol{v}_0 = \boldsymbol{v}_0 - \tilde{\boldsymbol{v}}(1) \tag{21}$$

$$\boldsymbol{D}_u\boldsymbol{F}^c(\boldsymbol{u}_0, \lambda)\cdot\boldsymbol{v}_0 = \boldsymbol{J}^c\cdot\boldsymbol{v}_0 = \boldsymbol{v}_0 - \boldsymbol{v}(2) \tag{22}$$

Substitution of Eqs. 21 and 22 into 20 gives for a bifurcation from symmetric period-1 states

$$\mu\boldsymbol{v}_0 = \tilde{\boldsymbol{v}}(1) \tag{23}$$

and for a bifurcation from asymmetric period-1 states

$$\mu\boldsymbol{v}_0 = \boldsymbol{v}(2). \tag{24}$$

The different dynamic bifurcations (symmetry-loss, bifurcation to quasi-periodic or q-periodic solutions) are obtained for the corresponding μ-values. We iterate the solution until we find the $\boldsymbol{v}_0$, which satisfies either Eqs. 23 or 24 for the specific μ value of the bifurcation of interest. The vectors $\tilde{\boldsymbol{v}}(1)$ and $\boldsymbol{v}(2)$ are the solutions of the linearized model equations integrated over one or two flowing periods, that is, the solution of

$$\frac{Le}{\sigma}\frac{\partial v_1}{\partial \tau} - \frac{1}{\phi_h^2}\frac{\partial^2 v_1}{\partial \xi^2} + \frac{f}{Da}\frac{\partial v_1}{\partial \xi} - \beta\cdot\left[\frac{\partial B}{\partial \Theta}\cdot v_1\cdot(1-x) - B(\Theta)\cdot v_2\right] + \Delta\cdot v_1 = 0$$

$$\frac{\epsilon}{\sigma}\frac{\partial v_2}{\partial \tau} - \frac{1}{\phi_m^2}\frac{\partial^2 v_2}{\partial \xi^2} + \frac{f}{Da}\frac{\partial v_2}{\partial \xi} - \frac{\partial B}{\partial \Theta}\cdot v_1\cdot(1-x) + B(\Theta)\cdot v_2 = 0 \tag{25}$$

subject to the spatial boundary conditions

$$\frac{Da}{\phi_h^2}\frac{\partial v_1}{\partial \xi} = v_1, \quad \frac{Da}{\phi_m^2}\frac{\partial v_2}{\partial \xi} = v_2 \quad \text{at} \quad \xi = 0 \tag{26}$$

$$\frac{\partial v_1}{\partial \xi} = 0, \quad \frac{\partial v_2}{\partial \xi} = 0 \quad \text{at} \quad \xi = 1 \tag{27}$$

and the initial condition

$$\boldsymbol{v}(\tau = 0) = \boldsymbol{v}_0. \tag{28}$$

Since an eigenvector is defined only up to a multiplicative constant, we assign an arbitrary value to one element or the norm of the vector, which is an additional equation. When μ and $\boldsymbol{v}_0$ are complex (bifurcation to quasi-periodic states), we integrate separately the real and complex parts of the equations.

Consequently, each singular point described above is determined by the residual Eqs. 12 or 13, the bifurcation conditions Eqs. 23 or 24 with the corresponding eigenvalue μ, as well as the choice of the norm of the eigenvector. These $2n+1$ equations define the $2n$ variables $(\boldsymbol{u}_0, \boldsymbol{v}_0)$ and λ at the singular points. The numerical method (shooting and Broyden's method) used to solve for the state and eigenvectors is described by Khinast and Luss (1997). All singular points were tracked with respect to an additional parameter by using a quasi arc length continuation scheme (Seydel and Hlavacek, 1987). Following the terminology of the singularity theory with a distinguished parameter (Golubitsky and Schaeffer, 1985), we define the codimension of a singular point to be 0 if it depends only on the bifurcation parameter λ. Note that in the nonlinear dynamics literature, these singular points are often defined to be of codimension 1.

Period-q states emerge when a complex pair of eigenvalues crosses the unit circle at angles of φ, such that

$$\varphi = 2\pi p/q, \tag{29}$$

with p and q being integers. Note that, for a large q, motion is indistinguishable from a quasi-periodic one. Two parameters have to be changed so that a pair of Floquet multipliers crosses the unit circle at $\varphi = 2\pi p/q$. The first parameter causes the crossing of the unit circle, the second one is needed to cross the unit circle exactly at $\varphi = 2\pi p/q$, that is, at the bifurcation point to q-periodic solutions. Therefore, bifurcations to period q ($q > 2$) are of codimension 1 (codimension 2 in the nonlinear dynamics literature). A codimension-1 bifurcation from symmetric to period-q ($q > 2$) states has to satisfy Eqs. 3 and 23, as well as

$$\mu_R = \cos(2\pi p/q) \quad \text{and} \quad \mu_I = \sin(2\pi p/q). \tag{30}$$

Additionally, a norm of the (complex) eigenvector has to be chosen. These equations determine $(\boldsymbol{u}_0, \boldsymbol{v}_0)$, λ and a parameter p_1 in $\boldsymbol{p}$.

The region of stable period-q solutions on the outside of the unit circle is called an Arnold resonance tongue (Arnold, 1983; Peckham et al., 1995). The boundaries of Arnold resonance tongues may be determined by the method described above. However, in order to track the boundaries the integration has to be performed over $2\cdot q$ flow-reversals (q cycles). The tip of the Arnold resonance tongue lies on the unit circle at $\varphi = 2\pi p/q$.

Other singular points of codimension 1 exist either at a tangential or transversal intersection of loci of codimension 0 singularities. Five types of different codimension-1 dynamic singularities were found in our study of the cooled RFR. Figure 6 describes their unfolding, that is, the two qualitatively different bifurcation diagrams obtained following a small perturbation of a parameter close to the singular point.

A *Bogdanov-Takens* (BT) bifurcation occurs when a quasi-periodic bifurcation exists at a limit point of the asymmetric solution, that is, at the intersection of the L-AS (limit point of asymmetric states) and the QP-AS (bifurcation between QP and AS states). At that point M^c has a double eigenvalue of $+1$.

A *Twist* (TW) bifurcation is formed at the intersection of the SL loci (symmetry loss of symmetric states) and a limit point of either the symmetric or asymmetric states, that is, L-S or L-AS. At this point M^s has one eigenvalue of $+1$ and one of -1.

We define a QPS singularity to be a point at which both an SL bifurcation and a QP-AS bifurcation occur so that M^c has a double eigenvalue of $+1$. Crossing this point shifts the sequence of stable stages in the bifurcation diagram from S $\rightarrow$ AS $\rightarrow$ QP to S $\rightarrow$ QP (see Figures 6g and 6h).

A *degenerate quasi-periodic bifurcation* (DQP) is a limit point of the QP locus. On one side of it, quasi-periodic states exist, and none exist on the other side. Here the condition (Eq. 19) has to be satisfied and, in addition, the derivative of the absolute value of the eigenvalue with respect to the bifurcation parameter vanishes, that is,

$$\frac{d(\mu_R^2 + \mu_I^2)}{d\lambda} = 0 \tag{31}$$

The computation of this point is more intricate than that of other singular points of codimension 1 and is described in the Appendix. At a *degenerate symmetry-loss* (DSL) bifurcation, the SL locus has a limit point so that a branch of asymmetric states exists only on one side of the point.

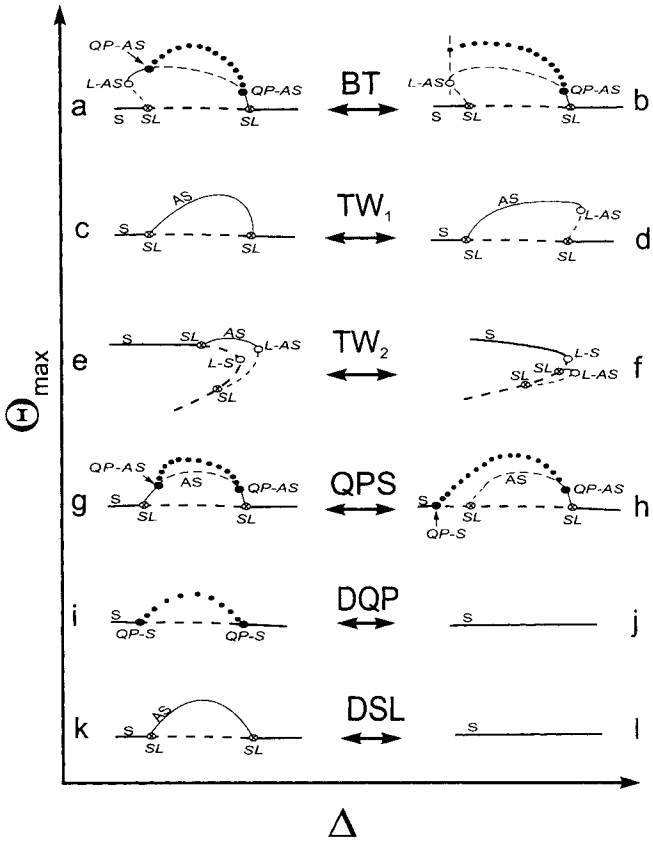

Figure 6. Bifurcation diagrams following unfolding of various codimension-1 singular points observed in our simulations.

S (AS) = symmetric (asymmetric) states; ●●● = quasi-periodic states; SL = symmetry loss; QP-S (-AS) = quasi-periodic bifurcation from symmetric (asymmetric) states; L-S (-AS) = limit points of symmetric (asymmetric) states.

Influence of Cooling and Cycle Time on the Dynamic Features

The method described above was used to construct a map (Figure 7) of regions with qualitatively different stable, periodic states for the example considered in this work. The boundaries separating regions with qualitatively different dynamic features are the loci of various codimension-0 singularities. These were computed only for flow-reversal periods exceeding 0.1 s, which is much shorter than that at which an RFR may be operated. Numerical difficulties precluded accurate calculations at shorter flow-reversal periods. Moreover, some of the assumptions of the pseudo-homogeneous model become questionable at this high flow-reversal frequency.

A typical dependence of the maximum temperature on the cooling capacity was shown in Figure 2 for a case where only symmetric and quasi-periodic states exist. The intermediate branch of the symmetric states is always unstable, while the extinguished branch is always stable. As shown in Figure 2, the branch of extinguished states emanates from a bifurcation point with negative cooling capacity and exists for all

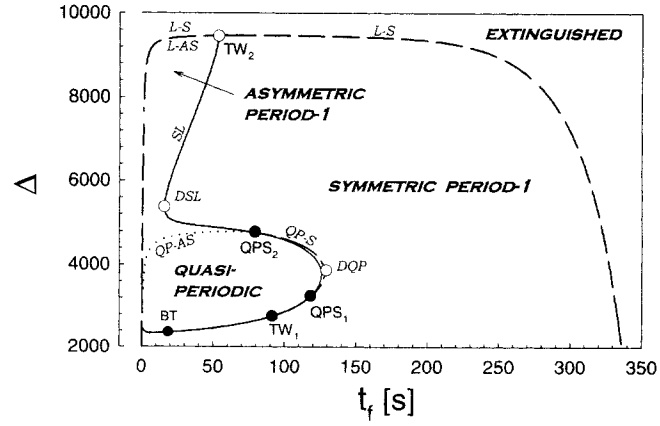

Figure 7. Map of regions with qualitatively different dynamic behavior of an RFR.

Boundaries are loci of codimension-0 singularities in the Δ-t_f plane. (SL = symmetry-loss; L-S = limit point of the symmetric solution; L-AS = limit point of the asymmetric solution; QP-S = quasi-periodic bifurcation of the symmetric solution; BT = Bogdanov-Takens bifurcation; DQP = degenerate quasi-periodic bifurcation; DSL = degenerate symmetry-loss bifurcation; TW = twist bifurcation; QPS = QPS bifurcation).

non-negative Δ values. Thus, in Figure 7 a stable extinguished, period-1 symmetric state exists for any t_f and cooling capacity. Figure 7 shows that only extinguished states are attained when either the cooling capacity exceeds a critical value or the flow-reversal time is either very long or very short. The reason is that when t_f is very large, the temperature front exits the reactor before the flow direction is reversed. When t_f is smaller than the characteristic reaction time, the conversion and heat generation in the reactor are negligible and only an exitinguished periodic state exists. We shall later compare and discuss the predictions of this model with those of the limiting model for infinitely high flow-reversal frequency.

Figure 7 shows that the loci of the limit points of the symmetric (L-S) and asymmetric (L-AS) period-1 states bound a region in which the RFR has ignited states in addition to the extinguished ones. The period-1 symmetric states occupy the largest part of this region of feasible operation and are the only ignited states that exist when the cooling and heat loss are insignificant. However, when the reactor is cooled complex periodic and asymmetric states exist for a rather large set of operating conditions. Asymmetric states exist for relatively high cooling capacities and short flow-reversal periods. The transition from symmetric to asymmetric states upon a decrease in t_f occurs via a SL bifurcation (line TW_2, DSL, QPS_2 in Figure 7). The quasi-periodic states exist for intermediate flow-reversal times and an intermediate level of cooling capacity. The symmetric period-1 states transform to quasi-periodic states usually via a quasi-periodic symmetric (QP-S) bifurcation. The line QPS_2, DQP, QPS_1 is a locus of such a bifurcation. The asymmetric period-1 states transform to quasi-periodic states at a quasi-periodic-asymmetric (QP-AS) bifurcation. However, in some cases, such as in the section between QPS_1 and BT, this transition is more intricate and consists of a sequence of several bifurcations. Since the loci of some of these bifurcations are very close to each other, it is not possible to distinguish among them in Figure 7. A more detailed map of part of the (Δ, t_f) plane is presented in Figure 8 that also includes an insert showing these bifurcations. Between TW_1 and BT, the symmetric and quasi-periodic states are separated by a very narrow (dashed) region, in which both symmetric and asymmetric states exist, followed by another narrow region (between QP-AS and SL) where only asymmetric states exist.

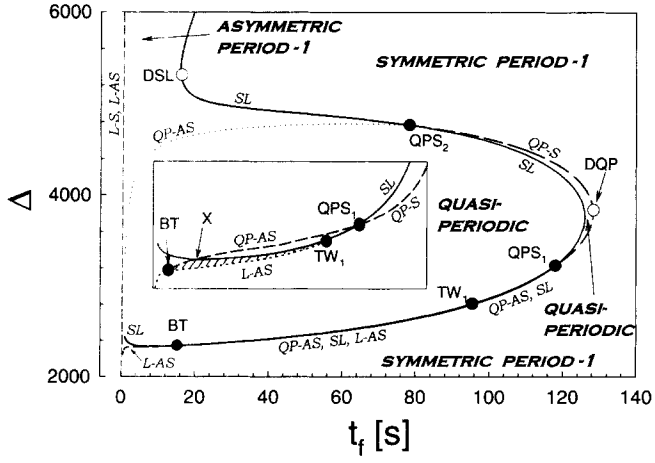

Figure 8. Enlarged map of regions with qualitatively different dynamic behavior of an RFR.

The insert is the region close to BT, TW_1 and QPS_1; both symmetric and asymmetric stable period-1 states coexist in the dashed region in the inset.

Figure 6 is a description of the various bifurcations that occur in this example. Some of the symmetric states on the ignited branch may be destabilized due to the supercritical or subcritical emergence of branches of asymmetric period-1 states (at SL points such as in Figures 6c–6d) or of a quasi-periodic branch (at QP-S points such as in Figure 6i). In some cases a branch of quasi-periodic states emerges from the branch of asymmetric states (QP-AS points). When a subcritical bifurcation of an asymmetric branch occurs, then for a certain range of Δ values (between SL and L-AS in Figure 6d) both symmetric and asymmetric period-1 stable states exist. This behavior was observed for the parameters bounded in the dashed region (TW_1, X, BT) in the insert in Figure 8. When the limit point of the asymmetric states is at a Δ value exceeding that of the limit point of the symmetric states then asymmetric ignited states exist for a range of Δ values (between L-S and L-AS in Figure 6e) in which no symmetric period-1 solution exists. In these cases the L-S locus does not bound the parameter region in which nonextinguished states exist. This behavior occurs in a very narrow region of parameters to the left of TW_2 in Figure 7. Due to the close proximity of the L-S and L-AS in this case, this narrow region cannot be detected in this map.

The intersections of the codimension-0 loci (SL, L-S, L-AS, QP-S, QP-AS) are codimension-1 singular points. As seen from Figures 7 and 8, the following codimension-1 singular points exist in our example: A Bogdanov-Takens (BT) point at the intersection of the L-AS and QP-AS, two Twist points at the intersection of the SL and the L-S or L-AS loci, and two QPS points at the tangential intersection of the QP-S and SL loci. The SL locus between the two QPS points is not observable as stability is lost at the QP-S points at which a quasi-periodic branch emerges. The degenerate quasi-periodic (DQP) bifurcation point is the largest flow-reversal period for which quasi-periodic states exist (see Appendix). In addition, the map includes the codimension-1 degenerate stability loss (DSL) point. Figure 6 shows the changes in the bifurcation diagrams upon the unfolding (perturbations) of such singular points.

As may be seen in Figures 7 and 8, the exotic asymmetric and quasi-periodic states tend to appear for relatively high flow-reversal frequencies. This is illustrated by Figure 9, which shows the emergence of asymmetric and quasi-periodic states as the flow-reversal period is decreased. Our calculations revealed a rather moderate change in the behavior of the RFR following a supercritical SL bifurcation. However, crossing the QP-S loci caused a rapid change in the qualitative dynamic features. The time series of the reactor center temperature (Figure 10) illustrates such a sharp transition. While a period-1 symmetric state exists for t_f of 129 s, a complex quasi-periodic state is obtained for t_f of 127 s. The real and imaginary parts of the conjugate complex eigenvalues change smoothly along the loci of the QP-S and QP-AS as the flow-reversal period and cooling capacity change. This leads to a continuous change of the oscillation frequency, which differs from the forcing (flow-reversal) frequency.

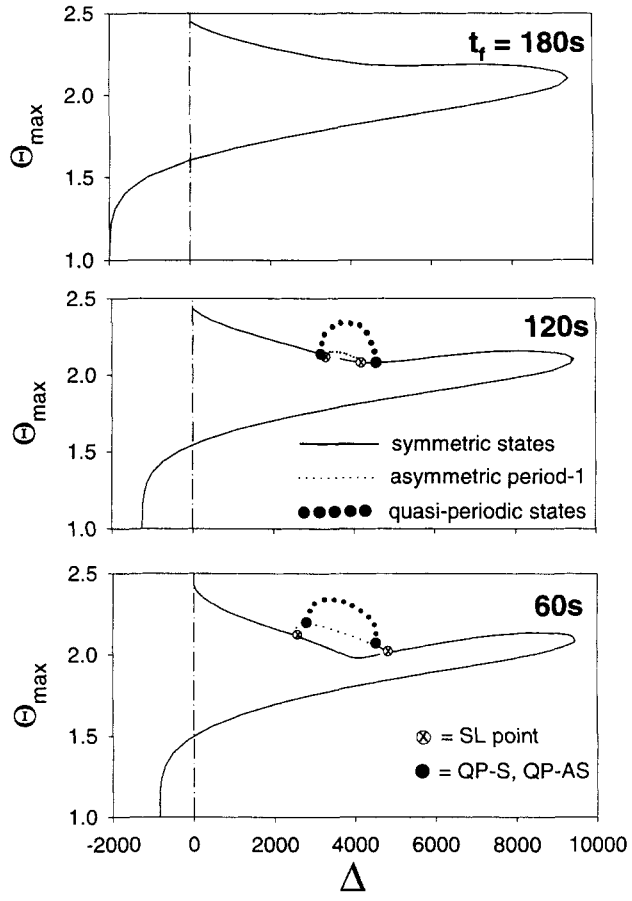

Figure 9. Emergence of asymmetric and quasi-periodic states upon decreasing the flow-reversal period.

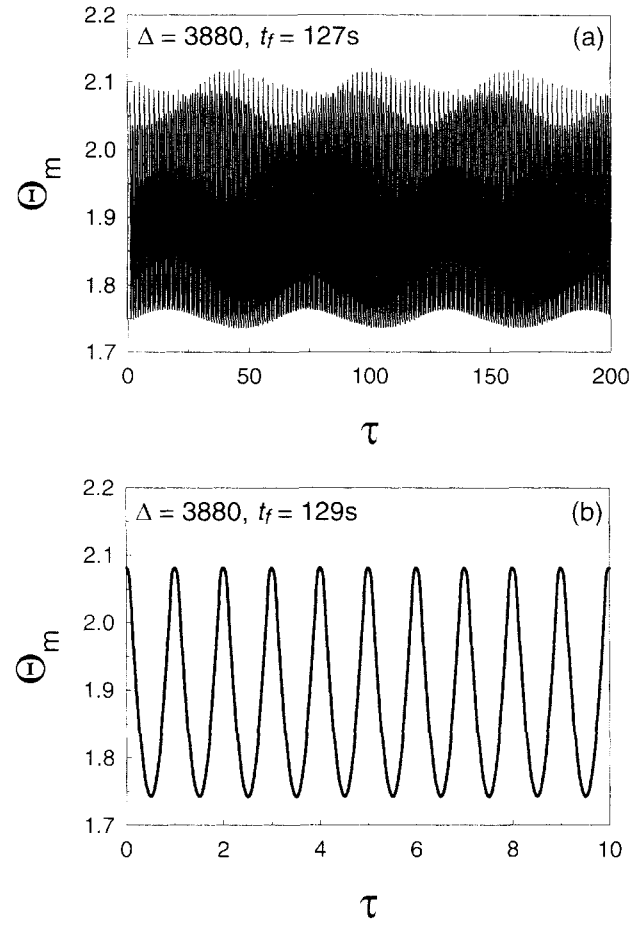

Figure 10. Changes between (b) symmetric period-1 to (a) quasi-periodic behavior of the temperature at the center of the RFR upon crossing the QP-S bifurcation.

In our example we did not observe any period-q ($q > 1$) bifurcation. Although in the general case of quasi-periodic bifurcations two noncommensurate periods (flow-reversal and the oscillation period) exist, one can expect that period-q states with a high period may exist for some parameter sets. It is rather difficult to distinguish between these and a quasi-periodic state since motions with high q values are in practice very similar to quasi-periodic ones. It should be noted that period-q motions may occur in a cooled RFR. In fact, Rehacek et al. (1992, 1998) found period-6 and -11 states interspersed in a region of aperiodic behavior. The mapping of period-q regions via continuation methods may be accomplished by an extension of the methods described in this study. However, it is more intricate to compute these bifurcations since the numerical effort is larger, as the equations have to be integrated over q periods. To determine the boundaries of the Arnold resonance tongues, it is best to find first such a state. Continuation techniques can then be used to reach the boundary of the region, and then to determine the region boundaries with the methods described above.

Limiting Model for Very Fast Flow Reversals

We now examine the dynamic features of the countercurrent flow reactor with it used as the limiting model for very high flow-reversal frequencies. Boreskov et al. (1983) and Matros (1989) pointed out that for very rapid flow reversals the temperature profile of the RFR approaches that of a countercurrent reactor with equal feed flow rates and velocities in the two directions. That limiting model simplifies significantly the prediction of the temperature profiles of the RFR at high flow-reversal frequencies and has been used by many investigators. Recent examples are articles by Nieken et al. (1995), Matros and Bunimovich (1996), and Somani et al. (1997). This model assumes that the axial temperature in both compartments is independent of the flow direction and the "averaged" energy balance is

$$\frac{1}{\phi_h^2}\frac{\partial^2\Theta}{\partial\xi^2} + \beta\cdot B(\Theta)\cdot 0.5\cdot[(1-x_1)+(1-x_2)] - \Delta\cdot(\Theta-\Theta_c) = 0 \quad (32)$$

The corresponding species balances are

$$\frac{1}{\phi_m^2}\frac{\partial^2 x_1}{\partial\xi^2} - \frac{1}{Da}\frac{\partial x_1}{\partial\xi} + B(\Theta)\cdot(1-x_1) = 0 \quad (33)$$

$$\frac{1}{\phi_m^2}\frac{\partial^2 x_2}{\partial \xi^2}+\frac{1}{Da}\frac{\partial x_2}{\partial \xi}+B(\Theta)\cdot(1-x_2)=0 \qquad (34)$$

where x_1 and x_2 are the conversion in the two countercurrent flow compartments. It is customary to assume that the model solutions are symmetric. We shall check if and when this *a priori* assumption is valid using the general boundary conditions

$$\frac{Da}{\phi_h^2}\frac{\partial \Theta}{\partial \xi}=\frac{1}{2}(\Theta-1),\quad \frac{Da}{\phi_m^2}\frac{\partial x_1}{\partial \xi}=x_1,\quad \frac{\partial x_2}{\partial \xi}=0 \quad \text{at } \xi=0 \qquad (35)$$

$$\frac{Da}{\phi_h^2}\frac{\partial \Theta}{\partial \xi}=-\frac{1}{2}(\Theta-1),\quad \frac{Da}{\phi_m^2}\frac{\partial x_2}{\partial \xi}=-x_2,\quad \frac{\partial x_1}{\partial \xi}=0 \quad \text{at } \xi=1. \qquad (36)$$

Two symmetry loss points from which asymmetric solutions emerge were found on the branch of the symmetric solutions of this limiting model (Figure 11). The asymmetric solutions existed within a bounded region of cooling capacities. The bifurcation of this branch of solutions was subcritical at Δ = 2,300 and supercritical at Δ = 4,960. Figure 12 shows the profiles of the symmetric and asymmetric states for a cooling capacity of Δ = 2,280, that is, in the region, where asymmetric and stable symmetric solutions coexist. Clearly, there exists another asymmetric state, which is a mirror image of the one shown. The example points out that assuming that the solutions of the limiting model are always symmetric may lead to pitfalls in simulations of a cooled RFR. Moreover, this limiting model does not predict correctly the behavior of the full model in the limit of very frequent flow reversals. The complete RFR model predicts that in the limit of $t_f \to 0$ only an extinguished state exists, while the ignited states of the limiting model do not depend on t_f.

Discussion and Conclusions

Cooling of an RFR may be required to avoid catalyst damage and deactivation or product degradation. Additionally, in laboratory and pilot-plant RFRs it is difficult to avoid heat losses. The examples presented here show that cooling of an RFR as in the case of a CSTR may lead to complex dynamic features, which are not exhibited by an adiabatic reactor. The transition from one type of periodic behavior to the other may be rather abrupt, as illustrated by Figure 10. The map of the various regions (Figure 7) shows that while the symmetric period-1 state is the most common ignited state, asymmetric and quasi-periodic states exist over an appreciable region of operating conditions. The aperiodic and asymmetric states certainly complicate the operation and control of an RFR and are undesirable since they usually lead to a maximum temperature exceeding that of symmetric period-1 states (see Figures 2 and 11). This excessive temperature rise may cause deactivation of the catalyst and lead to reactor safety problems. Thus, it is essential to be able to predict *a priori* when these undesired states occur.

The existence of the asymmetric and quasi-periodic states is associated with the inability of the bed temperature to

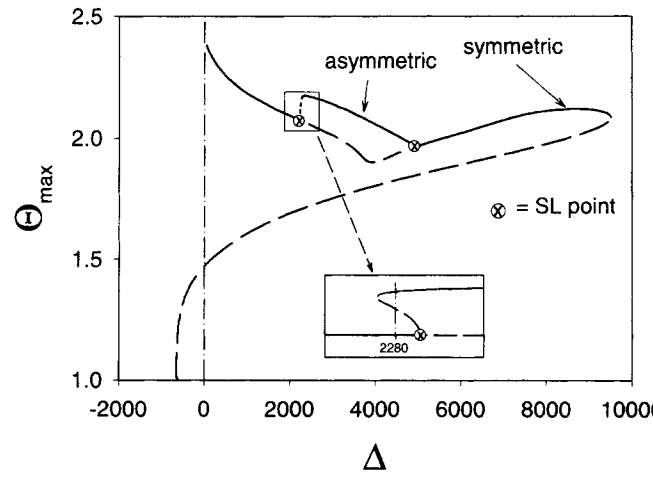

Figure 11. Dependence of the maximum temperature on the cooling capacity of a countercurrent reactor.

respond rapidly to the fast changes in the flow direction. Therefore, increasing the flow-reversal period above a critical value can eliminate these undesired states. The quasi-periodic behavior may be transformed to either symmetric or asymmetric period-1 states by a sufficient increase in the value of the cooling capacity. There are some very narrow regions of operating conditions in which a cooled RFR has two different stable ignited states, that is, a symmetric and an asymmetric state. At least in the example studied here, these parameter regions are very small and this interesting dynamic feature is mainly of academic interest and rather unlikely to be observed in practice. We did not observe any period doubling or any period-q ($q > 1$) motion in the example investigated here. However, Rehacek et al. (1992, 1998) found period-6 and -11 states interspersed in a region of aperiodic behavior for a different reaction system.

Moderate reactor cooling or heat losses are manifested by the existence of two local maxima in the temperature profile, similar to those found in our simulations (Figures 3b and 3c).

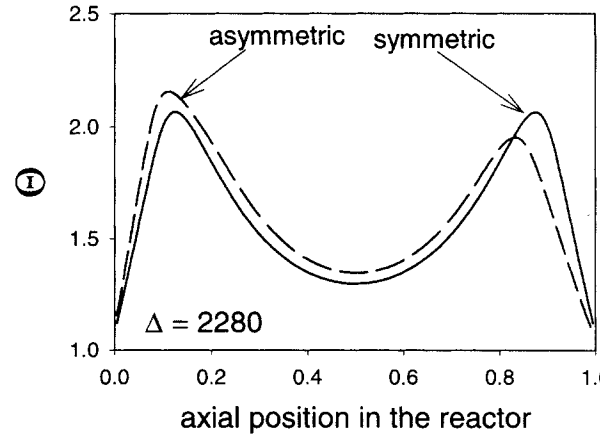

Figure 12. Temperature profiles of the symmetric and asymmetric states of the countercurrent reactor, which coexist for the same set of parameters (Δ = 2,280).

Time-averaged asymmetric profiles were reported in a recent experimental study by Züfle and Turek (1997) with no comments about the origin of the asymmetry. These asymmetric profiles with two local temperature maxima were observed only for high-temperature states, at which obviously heat loss was not negligible. Our results suggest that it is important to check whether cooling or heat loss to the surrounding area may generate the reported dynamic features in a particular reactor.

The finding of the asymmetric solutions for the limiting model for very high flow-reversal frequencies indicates that the common assumptions that this model has only symmetric states may lead to pitfalls. Thus, it is essential to solve that model with the boundary conditions given by Eqs. 35 and 36. It is of interest to note that the full model predicts that, for very frequent flow reversals, the RFR can attain only an extinguished state. The limiting model predicts, on the other hand, that the RFR may have symmetric and asymmetric ignited states in addition to the extinguished one. This shows that the limiting model has to be applied carefully. It should, however, be pointed out that this deviation occurs only when one considers the case of extremely high and impractical flow-reversal frequencies.

The mathematical procedure presented here enables an efficient, systematic mapping of parameter regions (Figures 7 and 8) in which a cooled RFR attains qualitatively different dynamic features. Specifically, it enables bounding of regions in which the cooled RFR has either symmetric states, asymmetric period-1 states, or quasi-periodic states. Applying these techniques together with those presented previously (Khinast and Luss, 1997) for determining all the multiplicity features of the RFR provides essential information for the rational design, operation, and control of this reactor. The high numerical efficiency of the procedure makes it feasible to routinely conduct this analysis in the design of an RFR. The computational techniques developed here for mapping the dynamic regions of an RFR may be applied also in the analysis of other periodic processes of distributed parameter systems, such as pressure swing adsorption (Kikkinides et al., 1995).

Acknowledgments

We gratefully acknowledge the financial support by the ACS-PRF and Mobil Foundation. We are most thankful to Prof. G. Auchmuty, Prof. V. Balakotaiah, and Prof. M. Golubitsky for many helpful discussion.

Notation

a_v = specific surface area, m^2/m^3
A_h = heat exchange area, L/m
$B(\Theta)$ = temperature dependence of reaction rate
c = concentration, $kmol/m^3$
c_p = heat capacity, J/(kg·K)
Da = Damköhler number, defined by Eq. 5
D_{ax} = axial diffusion constant, m^2/s
E_a = activation energy, J/mol
F = residual function
h = heat-transfer coefficient between fluid and catalyst, W/(K·m^2)
$-\Delta H$ = heat of reaction, J/mol
k_c = mass-transfer coefficient, m/s
k_∞ = frequency factor, L/s
$k(T_0)$ = rate constant at T_0, L/s
L = reactor length, m
Le = Lewis number, defined by Eq. 5
n = number of discretized state variables (2N)
N = number of node points
$\boldsymbol{p}$ = vector of parameters
r = outer reactor radius, m
R = universal gas constant, J/(mol·K)
t = time, s
t_c = cycle time (2 flow reversals), s
T = temperature, K
T_c = cooling temperature, K
ΔT_{ad} = adiabatic temperature rise, $-\Delta H c_0/(\rho c_p)_g$, K
u = superficial gas velocity, m/s
U = overall heat-transfer coefficient, W/(K·m^2)
v_0 = eigenvector of $\boldsymbol{J}$
y_0 = adjoint eigenvector of $\boldsymbol{J}$
z = axial coordinate, m
β = dimensionless adiabatic temperature rise, defined by Eq. 5
γ = dimensionless activation energy, defined by Eq. 5
ϵ = bed voidage
λ_s = solid conductivity, W/(m·K)
λ_{sg} = contribution of gas-solid heat transfer to λ_{ax}
ξ = dimensionless axial position, defined by Eq. 4
ρ = density, kg/m^3
σ = dimensionless reference time, defined by Eq. 5
τ = dimensionless time, defined by Eq. 4
φ = angle of the eigenvalues
ϕ_h^2 = heat transport modulus, defined by Eq. 5
ϕ_m^2 = mass transport modulus, defined by Eq. 5
Ψ = gas to solid volumetric heat capacity ratio, defined by Eq. 5

Indices

g = gas phase
0 = feed

Literature Cited

Arnold, V. I., *Geometrical Methods in the Theory of Ordinary Differential Equations*, Springer-Verlag, New York (1983).
Bhatia, S. K., "Analysis of Catalytic Reactor Operation with Periodic Flow-Reversal," *Chem. Eng. Sci.*, **46**, 361 (1991).
Blanks, R. F., T. S. Wittrig, and D. A. Peterson, "Bidirectional Adiabatic Synthesis Gas Reactor," *Chem. Eng. Sci.*, **45**, 2407 (1990).
Bobrova, L. N., E. M. Slavinskaya, A. S. Noskov, and Y. S. Matros, "Unsteady-State Performance of NO_x Catalytic Reduction by NH_3," *React. Kinet. Catal. Lett.*, **37**, 267 (1988).
Boreskov, G. K., Yu. Sh. Matros, and O. V. Kiselev, "Catalytic Processes Carried Out Under Nonstationary Conditions: Thermal Front in a Fixed Bed of Catalyst," *Kinet. Catal.*, **20**(3), 773 (1979).
Boreskov, G. K., G. A. Bunimovich, Yu. Sh. Matros, O. V. Kiselev, and I. A. Zolotarski, *Doklady Akademii Nauk SSR*, 268, 646 (1983).
Boreskov, G. K., and Yu. Sh. Matros, "Unsteady-State Performance of Heterogeneous Catalytic Reactions," *Catal. Rev.-Sci. Eng.*, **25**, 551 (1983).
Chen, Y. C., and D. Luss, "Wrong-Way Behavior of Packed-Bed Reactors: Influence of Interphase Transport," *AIChE J.*, **35**, 1148 (1989).
Chumakova, N. A., and Yu. Sh. Matros, "Isolating Laminar-Flow Regimes with Periodic Sweep Reversal in a Fixed Catalyst Layer," *Teoreticheskie Osnovy Khimicheskoi Tekhnologii*, **25**, 369 (1991).
Coddington, E., and N. Levinson, *Theory of Ordinary Differential Equations*, McGraw-Hill, New York (1955).
Cottrell, F. G., "Purifying Gases and Apparatus Therefore," U.S. Patent 2,171,733 (June 21, 1938).
Croft, D. T., and M. D. LeVan, "Periodic States of Adsorption Cycles—I. Direct Determination and Stability," *Chem. Eng. Sci.*, **49**, 1821 (1994a).
Croft, D. T., and M. D. LeVan, "Periodic States of Adsorption Cycles—II. Solution Spaces and Multiplicity," *Chem. Eng. Sci.*, **49**, 1831 (1994b).
Deuflhard, P., E. Hairer, and J. Zugck, "One-Step and Extrapolation Methods for Differential-Algebraic Systems," *Numer. Math*, **51**, 1 (1987).

Eigenberger, G., and U. Nieken, "Catalytic Combustion with Periodic Flow Reversal," *Chem. Eng. Sci.*, **43**, 2109 (1988).
Frank-Kamenetskii, D. A., *Diffusion and Heat Transfer in Chemical Kinetics*, Princeton University Press, Princeton, NJ (1955).
Gogolides, E., H. H. Sawin, and R. A. Brown, "Direct Calculation of Time-Periodic States of Continuum Models of Radio-Frequency Plasmas," *Chem. Eng. Sci.*, **47**, 3839 (1992).
Golubitsky, M., and D. G. Schaeffer, *Singularities and Groups in Bifurcation Theory*, Vol. 1, Springer, New York (1985).
Gupta, V. K., and S. K. Bhatia, "Solution of Cyclic Profiles in Catalytic Reactor Operation with Periodic Flow Reversal," *Comput. Chem. Eng.*, **15**, 229 (1991).
Haynes, T. N., C. Georgakis, and H. S. Caram, "The Design of Reverse Flow Reactors for Catalytic Combustion Systems," *Chem. Eng. Sci.*, **50**(3), 401 (1995).
Iooss, G., and D. D. Joseph, *Elementary Stability and Bifurcation Theory*, 2nd ed., Springer, New York (1990).
Ivanov, Yu. V., A. S. Noskov, Yu. Sh. Matros, and G. A. Bunimovich, "Multiplicity of States in Catalytic Reactor with Periodic Reversal of Gas Mixture Flow," *Teoreticheskie Osnovy Khimicheskoi Tekhnologii*, **26**, 228 (1992).
Keller, H. B., "Numerical Solutions of Bifurcation and Nonlinear Eigenvalue Problems," *Applications of Bifurcation Theory*, P. H. Rabinowitz, ed., Academic Press, New York, p. 159 (1977).
Kevrekidis, I. G., R. Aris, and L. D. Schmidt, "The Stirred Tank Forced," *Chem. Eng. Sci.*, **41**, 1549 (1986).
Khinast, J., and D. Luss, "Mapping Regions with Different Bifurcation Diagrams of a Reverse Flow Reactor," *AIChE J.*, **44**, 2034 (1997).
Kikkinides, E. S., V. I. Sikavitsas, and R. T. Yang, "Natural Gas Desulfurization by Adsorption: Feasibility and Multiplicity of Myclic Steady States," *Ind. Eng. Chem. Res.*, **34**, 255 (1995).
Leis, J. R., and M. A. Kramer, "Odessa—An Ordinary Differential Equation Solver with Explicit Simultaneously Sensitivity Analysis," *ACM Trans. Math. Software*, **14**(1), 61 (1988).
Matros, Yu. Sh., *Catalytic Processes under Unsteady State Conditions*, Elsevier, Amsterdam (1989).
Matros, Yu. Sh., "Performance of Catalytic Processes under Unsteady Conditions," *Chem. Eng. Sci.*, **45**, 2097 (1990).
Matros, Yu. Sh., and G. A. Bunimovich, "Reverse-Flow Operation in Fixed Bed Catalytic Reactors," *Cat. Rev. Sci. Eng.*, **38**, 1 (1996).
Neophytides, S. G., and G. G. Froment, "A Bench Scale Study of Reversed Flow Methanol Synthesis," *Ind. Eng. Chem. Res.*, **31**, 1583 (1992).
Nieken, U., G. Kolios, and G. Eigenberger, "Fixed-Bed Reactors with Periodic Flow Reversal: Experimental Results for Catalytic Combustion," *Cat. Today*, **20**, 355 (1994).
Nieken, U., G. Kolios, and G. Eigenberger, "Limiting Cases and Approximate Solutions for Fixed-Bed Reactors with Periodic Flow Reversal," *AIChE J.*, **41**, 1915 (1995).
Peckham, B. B., C. E. Frouzakis, and I. G. Kevrekidis, "Bananas and Banana Splits: A Parametric Degeneracy in the Hopf Bifurcation of Maps," *Siam. J. Math. Anal.*, **26** (1995).
Pinjala, V., Y. C. Chen, and D. Luss, "Wrong-Way Behavior of Packed-Bed Reactors: II. Impact of Thermal Dispersion," *AIChE J.*, **34**, 1663 (1988).
Press, W. H., S. A. Teukolsky, W. T. Vetterling, and B. P. Flannery, *Numerical Recipes in Fortran*, Cambridge University Press, Cambridge (1992).
Rehacek, J., M. Kubicek, and M. Marek, "Modeling of a Tubular Reactor with Flow Reversal," *Chem. Eng. Sci.*, **47**(9–11), 2897 (1992).
Rehacek, J., M. Kubicek, and M. Marek, "Periodic, Quasiperiodic and Chaotic Spatiotemporal Patterns in a Tubular Catalytic Reactor with Periodic Flow Reversal," *Computer Chem. Eng.*, **22**, 283 (1998).
Salinger, A. G., and G. Eigenberger, "The Direct Calculation of Periodic States of the Reverse-Flow Reactor: 1. Methodology and Propane Combustion Results," *Chem. Eng. Sci.*, **51**, 4903 (1996a).
Salinger, A. G., and G. Eigenberger, "The Direct Calculation of Periodic States of the Reverse Flow Reactor: 2. Multiplicity and Instability," *Chem. Eng. Sci.*, **51**, 4915 (1996b).
Sapundzhiev, C., J. Chaouki, C. Guy, and D. Klvana, "Catalytic Combustion of Natural Gas in a Fixed Bed Reactor with Flow Reversal," *Chem. Eng. Commun.*, **125**, 171 (1993).
Seiler, H., and G. Emig, "Reduction-Oxidation-Cycling in a Fixed Bed Reactor with Periodic Flow Reversal," *Dynamics and Reaction Kinetics in Heterogeneous Catalysis*, Symp. Proc., Antwerpen, Belgium (1997).
Seydel, R., and V. Hlavacek, "Role of Continuation in Engineering Analysis," *Chem. Eng. Sci.*, **42**, 1281 (1987).
Snyder, J. D., and B. Subramaniam, "Numerical Simulation of a Periodic Flow Reversal Reactor for Sulfur Dioxide Oxidation," *Chem. Eng. Sci.*, **48**, 4051 (1993).
Somani, M., S. Viswanath, J. Khinast, and D. Luss, "Maximum Temperature in a Reverse-Flow Reactor with Two Independent Reactions," *Chem. Eng. Sci.*, **52**, 2483 (1997).
Subramanian, S., and V. Balakotaiah, "Classification of Steady-State and Dynamic Behavior of Distributed Reactor Models," *Chem. Eng. Sci.*, **51**, 401 (1996).
van de Beld, B., and K. R. Westerterp, "Air Purification by Catalytic Oxidation in a Reactor with Periodic Flow Reversal," *Chem. Eng. Technol.*, **17**, 217 (1994).
van de Beld, B., "Air Purification by Catalytic Oxidation in an Adiabatic Packed-Bed Reactor with Periodic Flow Reactor," PhD Thesis, Univ. of Twente, Enschede, The Netherlands (1995).
Vortmeyer, D., and R. J. Schaefer, "Equivalence of One- and Two-Phase Models for Heat Transfer Processes in Packed Beds: One Dimensional Theory," *Chem. Eng. Sci.*, **29**, 484 (1974).
Watson, E. W., "Method and Apparatus for Reacting for Sulfur Dioxide and Natural Gas," U.S. Patent 3,865,927 (1975).
Züfle, H., and T. Turek, "Catalytic Combustion in a Reactor with Periodic Flow Reversal: 1. Experimental Results," *Chem. Eng. Proc.*, **36**, 327 (1997).

Appendix

Computation of the monodromy matrix

The monodromy matrix is equal to the sensitivity matrix $S(\tau_f)$ at the end of the flowing period. The sensitivity matrix is defined as

$$S(\tau) = \left[\frac{\partial u(\tau)}{\partial u_1(0)}, \frac{\partial u(\tau)}{\partial u_2(0)}, \cdots, \frac{\partial u(\tau)}{\partial u_n(0)} \right] \tag{A1}$$

where u is the spatially discretized state vector. The discretized model has the form

$$\frac{\partial u}{\partial \tau} - f(u, \lambda, p) = 0 \qquad u(\tau = 0) = u_0 \tag{A2}$$

The sensitivity matrix is computed by differentiating Eq. A2 with respect to the initial conditions and integrating the set of $n \times n$ differential equations

$$\frac{dS}{d\tau} = A(u(\tau), \lambda, p) \cdot S \qquad S(\tau = 0) = I \tag{A3}$$

where A is the Jacobian matrix of f. The sensitivity matrix S may also be determined by computing $S^{(\tau + \Delta\tau)}$ at every time step from the Crank-Nicholson discretized form of Eq. A3, that is

$$S^{(\tau+\Delta\tau)} = \left[\frac{2}{\Delta\tau} I - A(\tau + \Delta\tau) \right]^{-1} \cdot \left(\frac{2}{\Delta\tau} I + A(\tau) \right) \cdot S^{(\tau)} \tag{A4}$$

We denote the monodromy matrix for a semicycle M^s, that is

$$M^s(u_0, \lambda_0) = \tilde{S}^s(\tau = 1) \tag{A5}$$

where the tilde means mirror reflection of the rows. The monodromy matrix computed by integration over the full cycle of two flow reversals ($\tau_c = 2$) is denoted as $\boldsymbol{M}^c$. Thus

$$\boldsymbol{M}^c(\boldsymbol{u}_0, \lambda_0) = \boldsymbol{S}^c(\tau = 2) \tag{A6}$$

Leis and Kramer (1988) developed a solver ODESSA based on LSODE for integration of the sensitivity (variational) equations together with Eq. A2. However, integrating Eq. A2 with LIMEX (Deuflhard et al., 1987) and simultaneously solving Eq. A4 was faster than using ODESSA at the same accuracy. However, we expect ODESSA's performance to be superior for more complicated problems due to the higher level of sophistication. The eigenvalues of $\boldsymbol{M}$ were calculated by the QR-algorithm routine RG in EISPACK (NETLIB). Because of the associated extensive computational effort, the $\boldsymbol{M}$'s were computed only in a few cases to check the validity of our stability predictions for some test cases.

Degenerate quasi-periodic (DQP) bifurcation locus

At a DQP point, the equations describing a quasi-periodic bifurcation are satisfied and in addition

$$\frac{d(\mu_R^2 + \mu_I^2)}{d\lambda} = 2\left[\mu_R \frac{d\mu_R}{d\lambda} + \mu_I \frac{d\mu_I}{d\lambda}\right] = 0 \tag{A7}$$

Direct computation of the derivative of the eigenvalues in Eq. A7 is rather complex. Another approach is to use the fact that the eigenvalues and eigenvectors of the monodromy matrix $\boldsymbol{M}$ satisfy the relation

$$\mu = \frac{\boldsymbol{y}^* \cdot \boldsymbol{M} \cdot \boldsymbol{v}}{\boldsymbol{y}^* \boldsymbol{v}} \tag{A8}$$

It may be shown that

$$\left.\frac{d\mu}{d\lambda}\right|_{u_0, \lambda} = \frac{\boldsymbol{y}^* \boldsymbol{M}_\lambda \boldsymbol{v}}{\boldsymbol{y}^* \boldsymbol{v}} \tag{A9}$$

where

$$\boldsymbol{M}_\lambda = \left.\frac{d(\boldsymbol{M}(\boldsymbol{u}_0, \lambda_0))}{d\lambda}\right|_{u_0, \lambda_0} \tag{A10}$$

is the total derivative of $\boldsymbol{M}$. Substitution of the relation $\boldsymbol{M} = \boldsymbol{I} - \boldsymbol{J}$ gives

$$\frac{d\mu}{d\lambda} = \frac{\boldsymbol{y}^*(\boldsymbol{I} - \boldsymbol{J})_\lambda \boldsymbol{v}}{\boldsymbol{y}^* \boldsymbol{v}} = -\frac{\boldsymbol{y}^* \boldsymbol{J}_\lambda \boldsymbol{v}}{\boldsymbol{y}^* \boldsymbol{v}} \tag{A11}$$

$\boldsymbol{J}_\lambda$ may be determined by

$$\frac{d\boldsymbol{J}}{d\lambda} \cdot \boldsymbol{v} = \left(\frac{d}{d\lambda} \boldsymbol{D}_u \boldsymbol{F}(\boldsymbol{u}, \lambda)\right) \cdot \boldsymbol{v}$$

$$= \boldsymbol{D}^2_{u\lambda} \boldsymbol{F}(\boldsymbol{u}, \lambda) \cdot \boldsymbol{v} + \boldsymbol{D}^2_{uu} \boldsymbol{F}(\boldsymbol{u}, \lambda) \cdot (\boldsymbol{b}, \boldsymbol{v}) \tag{A12}$$

where

$$\boldsymbol{b} = \frac{\partial \boldsymbol{u}}{\partial \lambda} \tag{A13}$$

With this, Eq. A11 becomes

$$\left.\frac{d\mu}{d\lambda}\right|_{u_0, \lambda_0} = -\frac{\boldsymbol{y}^* \cdot \left[\boldsymbol{D}^2_{u\lambda} \boldsymbol{F}(\boldsymbol{u}, \lambda) \cdot \boldsymbol{v} + \boldsymbol{D}^2_{uu} \boldsymbol{F}(\boldsymbol{u}, \lambda) \cdot (\boldsymbol{b}, \boldsymbol{v})\right]}{\boldsymbol{y}^* \boldsymbol{v}} \tag{A14}$$

$\boldsymbol{D}^2_{uu} \boldsymbol{F} \cdot (\boldsymbol{b}, \boldsymbol{v})$ and $\boldsymbol{D}^2_{u\lambda} \boldsymbol{F} \cdot \boldsymbol{v}$ may be determined by Fréchet differentiation of the model equations and integration of a set of ODEs. $\boldsymbol{b}$ may be computed by differentiating $\boldsymbol{F}(\boldsymbol{u}, \lambda) = 0$ with respect to λ, that is

$$\frac{d\boldsymbol{F}}{d\lambda} = \frac{\partial \boldsymbol{F}}{\partial \lambda} + \boldsymbol{J} \cdot \frac{\partial \boldsymbol{u}}{\partial \lambda} = \frac{\partial \boldsymbol{F}}{\partial \lambda} + \boldsymbol{J} \cdot \boldsymbol{b} = 0. \tag{A15}$$

The product of $\boldsymbol{J} \cdot \boldsymbol{b}$ is computed by integrating the linearized model equations Eqs. 25–27 with the initial condition $\boldsymbol{v}(0) = \boldsymbol{b}$. Equation A15 is used to iteratively determine $\boldsymbol{b}$. When Δ is selected as the bifurcation parameter

$$\frac{\partial \boldsymbol{F}}{\partial \lambda} = \begin{pmatrix} \Theta - \Theta_c \\ 0 \end{pmatrix}. \tag{A16}$$

The adjoint eigenvector $\boldsymbol{y}$ satisfies the equation

$$\boldsymbol{y}^* \boldsymbol{M}(\boldsymbol{u}_0, \lambda) = \mu \cdot \boldsymbol{y}^* \tag{A17}$$

Substitution of $\boldsymbol{M} = \boldsymbol{I} - \boldsymbol{J}$ into Eq. A17 gives

$$\boldsymbol{y}^*(\boldsymbol{I} - \boldsymbol{J}) = \mu \cdot \boldsymbol{y}^* \Rightarrow \boldsymbol{y}^* \boldsymbol{J} = (1 - \mu) \cdot \boldsymbol{y}^* \tag{A18}$$

Again only the product of $\boldsymbol{J}^* \cdot \boldsymbol{y}$ has to be evaluated by determining the adjoint operator of the linearization. The method of determining the adjoint eigenvector of the periodic states of the RFR was described by Khinast and Luss (1997). Since the eigenvector is only determined up to a multiplicative constant, we can assign an arbitrary value to one element in the vector. We choose an inner product between the eigenvector and the adjoint eigenvector

$$\langle \boldsymbol{v}, \boldsymbol{y} \rangle = 1 + i \tag{A19}$$

This guarantees that the numerical scheme does not converge to a trivial (zero) eigenvector or adjoint eigenvector. These conditions determine $\boldsymbol{u}$, $\boldsymbol{v}$, $\boldsymbol{y}$, μ_R, μ_1, λ and an additional parameter in $\boldsymbol{p}$.

Manuscript received Sept. 15, 1997, and revision received Feb. 9, 1998.